Dilead Structural Units in Lead Halide and Hydroxo/Oxo Molecules, Clusters, and Extended Structures Found in Molten Salts, Aqueous Solutions, and the Solid State

Lars A. Bengtsson*,† and Roald Hoffmann‡

Contribution from the Department of Inorganic Chemistry 1, University of Lund, P.O. Box 124, S-221 00 Lund, Sweden, and Department of Chemistry, Cornell University, Baker Lab, Ithaca, New York 14853-1301

Received August 7, 1992

Abstract: The dilead clusters Pb_2X^{3+} (X = F, Cl, Br, I) and $Pb_2(OH)_2^{2+}$ are stabilized by partial Pb–Pb bonding induced by bridging halide or hydroxide ions. The maximum Pb–Pb bonding (analyzed here with approximate molecular orbital calculations) is obtained in complexes with predominantly ionic lead–anion interactions. Larger lead hydroxo/oxo clusters in aqueous solution also seem to be stabilized by partial Pb–Pb bonding, but the structures of hydroxo/oxo clusters isolated in the solid state are dominated by Pb–O bonding. Only long Pb–Pb contacts are found, due to the lack of a stabilizing ionic medium. The $[(PbO)_2Cu]YSr_2Cu_2O_6$ family of high-T_c superconductors contains Pb_2O_2 layers encapsulating a Cu(I) layer. The Pb_2O_2 layers are brought close enough to allow strong interlayer Pb–Pb interaction, which significantly affects the compounds' structural and electronic properties. The effects of oxidation and cation substitution on these structures are also investigated. Strong analogies with the chemical bonding in dilead clusters are observed.

Introduction

The thermodynamics of formation and local structure of di- and polymetal complexes in ionic liquids and concentrated aqueous solution have been studied for various systems. Interest has focused on systems with $d^{10}s^2$ metal ion ligands, such as Tl^+, Pb^{2+}, and Bi^{3+}, coordinated to central anions, ranging from the hard donors F^- and OH^- to soft donors exemplified by Br^- and I^-.[1-6]

The dilead complexes show a tendency to form bridged species such as **1a** and **1b**. The thermodynamics of formation of these

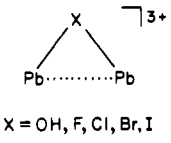

1a

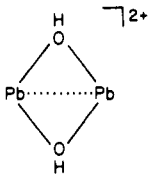

1b

complexes shows a pattern of $\Delta H° < 0$ and $\Delta S° < 0$. In light of the structures of these complexes, which show unusually short Pb–Pb contacts comparable to those in the pure metal and in Zintl anions such as Pb_5^{2-},[7-11] the thermodynamic results were interpreted in terms of significant attractive Pb–Pb bonding overcoming the obvious Coulombic Pb^{2+}–Pb^{2+} repulsion.

The planar $Pb_2(OH)_2^{2+}$ complex deserves special interest, since it constitutes, alongside the more frequently encountered edge-sharing Pb_4O tetrahedra,[4] a basic structure block which appears in many divalent lead hydroxo/oxo clusters and extended structures. The solid-state chemistry of divalent lead hydroxo/oxo compounds has been reviewed fairly recently.[4] Model systems for edge-sharing tetrahedra are the divalent α- and β-PbO, which already have been investigated theoretically by Trinquier and Hoffmann.[12] Even though the Pb–Pb contacts are fairly long in these compounds, it was shown that both intra- and interlayer Pb–Pb interactions are of significance for their structural and physical properties.

In this contribution, the bonding in the experimentally characterized complexes **1a** and **1b** is investigated on the extended Hückel level of approximate molecular orbital theory. The corresponding Tl_2Br^+ ion is also studied, due to its similarity and yet long metal–metal contact. The insights into the bonding scheme of the dilead complexes are then used to obtain a basic understanding of the bonding and electronic structures of lead hydroxo/oxo clusters as well as extended compounds containing planar Pb_2O_2 sheets. An intriguing family of solids which display such structural features belongs to a new type of high-T_c superconductors based on the parent structure of $[(PbO)_2Cu]$-$Sr_2YCu_2O_6$. A characteristic feature of this type of ceramics is an unusual PbO–Cu–PbO triple layer.[13]

Computations

All calculations in this work were performed within the framework of the extended Hückel method,[14,15] employing the usual Wolfsberg–Helmholz equation with $K = 1.75$ in order to calculate off-diagonal elements h_{ij}. The energy and radial parameters, h_{ii} and ζ_i, were taken from a selection of tested empirical parameters collected by Alvarez.[16] The empirical parameters for the heavy main-group elements turn out

† University of Lund.
‡ Cornell University.

(1) Bengtsson, L. A.; Holmberg, B. *J. Chem. Soc., Faraday Trans. 1* **1989**, *85*, 305–316.
(2) Bengtsson, L. A.; Holmberg, B. *J. Chem. Soc., Faraday Trans. 1* **1989**, *85*, 317–329.
(3) Bengtsson, L. A.; Holmberg, B. *J. Chem. Soc., Faraday Trans. 1* **1989**, *85*, 2917–2930.
(4) Bengtsson, L. A.; Holmberg, B. *J. Chem. Soc., Faraday Trans.* **1990**, *86*, 351–354.
(5) Holmberg, B.; Bengtsson, L. A.; Johansson, R. *J. Chem. Soc., Faraday Trans. 1* **1990**, *86*, 2187–2192.
(6) Bengtsson, L. A.; Frostemark, F.; Holmberg, B., to be published.
(7) Corbett, J. D.; Edwards, P. A. *J. Chem. Soc., Chem. Commun.* **1975**, 984–985.
(8) Edwards, P. A.; Corbett, J. D. *Inorg. Chem.* **1977**, *16*, 903–907.
(9) Corbett, J. D. In *Chemistry for the Future*; Grünewald, H., Ed.; Pergamon Press: Oxford, 1984; pp 125–130.
(10) Neuburger, M. C. *Z. Kristallogr.* **1931**, *80*, 103–131; **1933**, *86*, 395–422; **1936**, *93*, 1–36.
(11) Steeb, S. *Z. Metallk.* **1961**, *52*, 422–425.
(12) Trinquier, G.; Hoffmann, R. *Inorg. Chem.* **1984**, *88*, 6696–6711.
(13) Cava, R. J.; Batlogg, B.; Krajewski, J. J.; Rupp, L. W.; Schneemeyer, L. F.; Siegrist, T.; vanDover, R. B.; Marsh, P.; Peck, W. F., Jr.; Gallagher, P. K.; Galrum, S. H.; Marshall, J. H.; Farrow, R. C.; Waszczak, J. V.; Hull, R.; Trevor, P. *Nature* **1988**, *336*, 211–214.
(14) Hoffmann, R. *J. Chem. Phys.* **1963**, *39*, 1397–1412.
(15) Hoffmann, R.; Lipscomb, W. N. *J. Chem. Phys.* **1962**, *36*, 2179–2189; *37*, 2872–2883.
(16) Alvarez, S., unpublished data, Barcelona, 1989.

0002-7863/93/1515-2666$04.00/0

Table I. Parameters Used in the Extended Hückel Calculations

atom	orbital	h_{ii}/eV	ζ_1	ζ_2	c_1	c_2
H	1s	−13.60	1.30			
N	2s	−26.00	1.95			
	2p	−13.40	1.95			
O	2s	−32.30	2.28			
	2p	−14.80	2.28			
F	2s	−40.00	2.42			
	2p	−18.10	2.42			
Cl	3s	−26.30	2.18			
	3p	−14.20	1.73			
Ca	4s	−5.34	1.07			
	4p	−3.57	0.89			
Cu	4s	−11.40	2.20			
	4p	−6.06	2.20			
	3d	−14.00	5.95	2.30	0.5933	0.5744
Br	4s	−22.07	2.59			
	4p	−13.10	2.13			
Sr	5s	−4.93	1.21			
	5p	−3.28	1.00			
Y	5s	−5.48	1.31			
	5p	−3.51	1.08			
I	5s	−18.00	2.68			
	5p	−12.70	2.32			
Tl	6s	−11.60	2.30			
	6p	−5.00	1.60			
Pb	6s	−15.70	2.35			
	6p	−8.00	2.06			
Bi	6s	−18.67	2.56			
	6p	−7.81	2.07			

to be very similar to the relativistic values calculated by Pyykkö and Lohr.[17] For this reason values from Pyykkö and Lohr were used whenever empirical ones could not be obtained. All parameters used in the calculations are shown in Table I.

The tight-binding approximation was used for extended structures.[18] The k points were chosen according to the guidelines of Ramirez and Böhm.[19]

The effect of relativistic contraction of the 6s orbitals of Tl, Pb, and Bi was probed by numerical experiments, repeating some calculations with ζ_i values of Pyykkö and Lohr.[17] Although a general down-scaling of all interaction was observed, no changes in Pb–Pb bonding relative to a reference bond was inferred. Therefore, such effects are not discussed further.

Dilead Complexes

A Standard Pb–Pb Bond. The Mulliken overlap population is a good indicator of partial metal–metal bonding, irrespective of the choice of parameters, as long as the bonding is referred to a standard or reference state.[20] We need to define such a standard Pb–Pb single bond.

In different tables the covalent radius of Pb is given as between 1.45 and 1.50 Å.[21] Considering this fact and the bond lengths of 3.0 and 3.2 Å in Pb_5^{2-},[7-9] a reasonable reference system is a hypothetical ethane analogue $H_3Pb–PbH_3$ with a Pb–Pb distance of 3.00 Å and a Pb–H distance of 1.80 Å.[22] The hydrogens are tetrahedrally arranged around each Pb. The Pb–Pb interaction in this molecule stems almost exclusively from a σ Pb(6s and 6p)–Pb(6s and 6p) overlap. The Mulliken overlap population works especially well as an indicator of bonding when the two atoms considered are identical by symmetry (or nearly so). It is less reliable for bonding between atoms of very different electronegativity. Whenever the latter type of interactions is surveyed in this work, only the relative changes with respect to a reference will be considered.

(17) Pyykkö, P.; Lohr, L. L., Jr. *Inorg. Chem.* **1981**, *20*, 1950–1959.
(18) Whangbo, M.-H.; Hoffmann, R.; Woodward, R. B. *Proc. R. Soc. London* **1979**, *366*, 23–46.
(19) Ramirez, R.; Böhm, M. C. *Int. J. Quantum Chem.* **1986**, *30*, 391–411; *34*, 571–594.
(20) Janiak, C.; Hoffmann, R. *J. Am. Chem. Soc.* **1990**, *112*, 5924–5946.
(21) Most textbooks in inorganic and structural chemistry provide such a table with the covalent radii of the most common elements, but rarely is any reference given.
(22) Pyykkö, P. *Chem. Rev.* **1988**, *88*, 563–594.

Table II. Experimental Geometries and Calculated Overlap Populations in Dilead Complexes

	X				
property	OH[a]	F[b]	Cl[b]	Br[b]	I[b,d]
d_{Pb-X}/Å	2.71	2.53	2.52	2.61	2.79
d_{Pb-Pb}/Å	3.40	3.40[c]	3.38	3.39	3.40
$\angle_{Pb-X-Pb}$/deg	78	84	84	81	75
Pb–Pb overlap population (case 1)/%[e]	19	21	11	14	21
Pb–Pb overlap population (case 2)/%[e]	17	20	9	12	17
Pb–X overlap population[f]	0.07 (×2)	0.06	0.51	0.51	0.25

[a] Experimental structure according to **1b** and **2b**. [b] Experimental structure according to **1a** and **2a**. [c] The Pb–Pb distance was set to 3.40 Å for sake of comparison. [d] Hypothetical structure with a typical Pb–I distance. [e] Percent of reference Pb–Pb overlap population in H_3PbPbH_3. [f] Reduced absolute values.

The Pb–Pb overlap population in $H_3Pb–PbH_3$ is 0.713. The Pb–Pb overlap populations discussed below will generally be given in percentages of this standard overlap population rather than their absolute values.

Solvent Effects. The highly charged species Pb_2X^{3+} and $Pb_2(OH)_2^{2+}$ are unlikely to exist in the gas phase without a supporting medium. The ionic liquid or concentrated aqueous solution has a stabilizing effect. In order to get a qualitative picture of the medium effect on the stability of the dilead complexes in general and a Pb–Pb bond in particular, calculations were performed for two specific cases: (1) The medium is considered as stabilizing in an undefined manner, i.e., the highly charged complexes are regarded as situated in a pocket or void of the host ionic liquid surrounded by solvent anions. The calculations were thus performed on the "naked" Pb_2X^{3+} and $Pb_2(OH)_2^{2+}$ ions shown in **1a** and **1b**. This approach represents an underestimation of the solvent effect. (2) All foreign cations so far investigated in molten nitrate media seem to be quasitetrahedrally coordinated by four nitrate ions in a flat-on asymmetric bidentate manner.[23] The shortest Pb–O(NO_2) distance is 2.38 Å. The nitrate coordination of Pb^{2+} was modeled by several oxide ions O^{2-} at 2.38 Å in a tetrahedral configuration, as seen in **2a** and **2b**. This

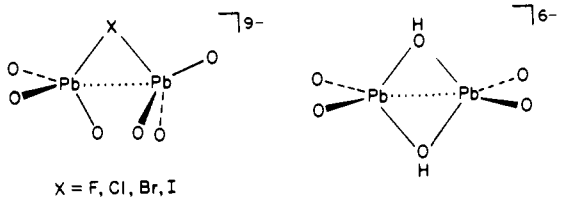

2a **2b**

geometry approximates that of the nitrate ion in its characteristic coordination mode. The electron donation and bonding, however, are probably exaggerated. This approach represents an overestimation of the solvent effect induced by the oxides. The three oxides coordinated and the X complete an approximate tetrahedron around each lead atom. The oxides on one of the lead atoms in **2a** are twisted 60° around the Pb–X bond with respect to the other lead atom in order to avoid an O^{2-}–O^{2-} interaction. The Pb^{2+} ions thus become unequal by symmetry, but the overall effects of this distortion are small.

Our general guideline in interpretations of results from the calculations is that any significant property observed for both cases 1 and 2 (vide supra) probably is a significant property of the molecular unit studied.

Partial Pb–Pb Bonding. The structural parameters of Pb_2X^{3+} (X = F, Cl, Br, I) and $Pb_2(OH)_2^{2+}$ used in the calculations are shown in Table II, together with the calculated Pb–Pb overlap populations. We will use the Pb_2Br^{3+} complex for a more detailed

(23) Bengtsson, L. A. Ph.D. Thesis, University of Lund, 1990, pp 47–54.

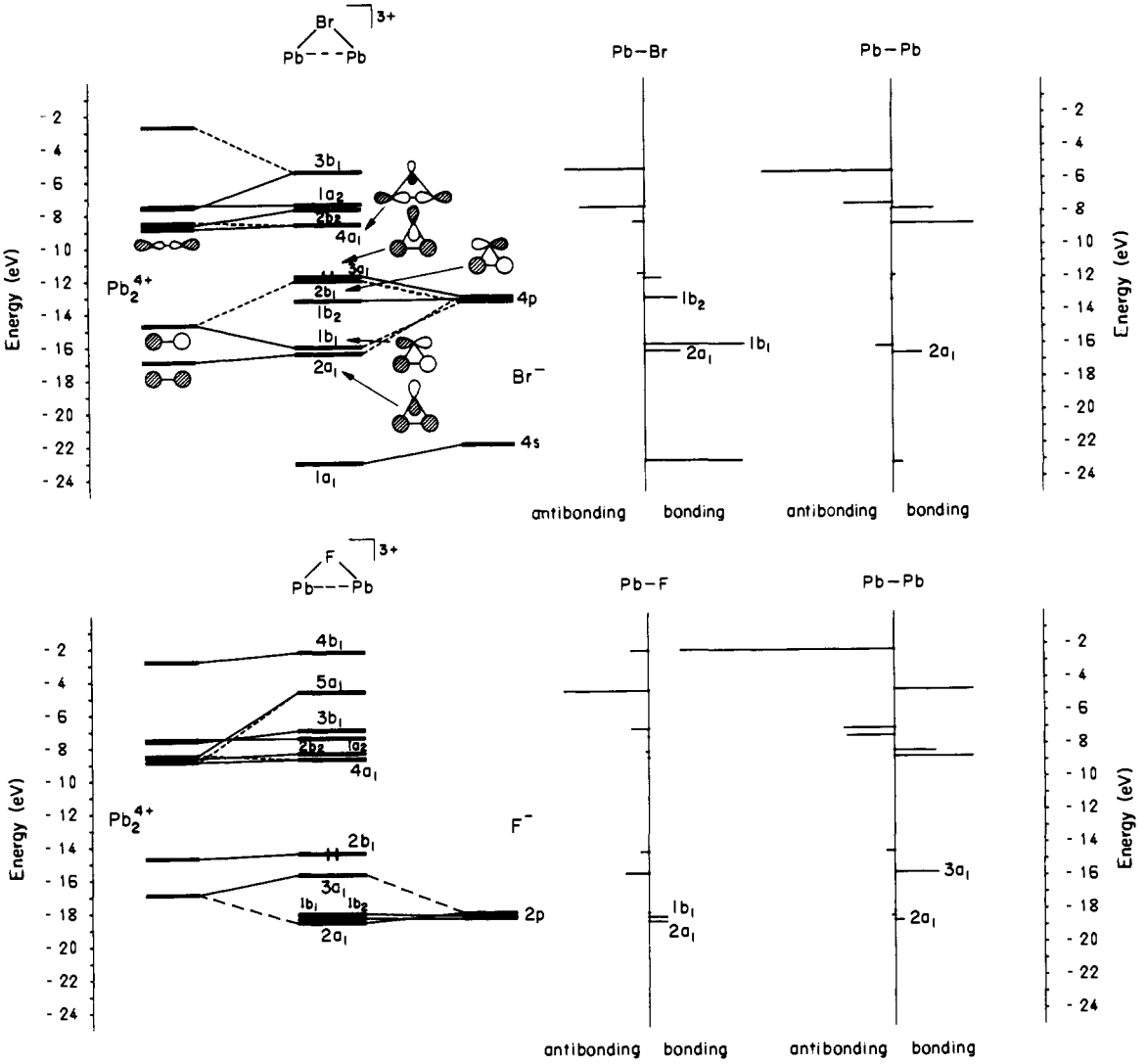

Figure 1. Energy diagrams and MOOP of the fragments Pb_2^{4+} and X^- (X^- = Br^- and F^-) forming Pb_2Br^{3+} and Pb_2F^{3+}, respectively.

analysis for two reasons. First, this is the dilead complex in which the effect of the central anion on the Pb_2^{4+} pair is most profound. Second, valuable comparisons can be made with the isoelectronic Tl_2Br^+, for which experimental thermodynamic and structural data also exist.[4,5]

The interaction diagrams, together with the molecular orbital overlap populations (MOOP), between a Pb_2^{4+} entity and Br^- and F^- are shown in Figure 1. The MOOP plot is a graphic way of showing the bonding characteristics of each MO. A line appears, positive to the right, negative to the left, whose length is proportional to the overlap for the specified bond. The main Pb–Pb bonding arises from Pb(6s and 6p)–Pb(6s and 6p) σ interactions from molecular orbitals (MOs) of a_1 symmetry. Population of the lowest unoccupied MO (LUMO) would increase significantly Pb–Pb bonding (56% of the standard bond). Even though such a reduction is highly unlikely in oxidizing molten salts such as the alkali nitrates, this type of interaction is the reason for the unusual stability of hypervalent Bi clusters in even more acidic melts (chloroaluminates).[24,25] Furthermore, it can be seen that the Pb–Pb bonding MOs actually are destabilized by the presence of the bromide ion. An overall gain in energy is, of course, obtained through the covalent (and Coulombic) Pb–Br bonding.

The main difference in Pb–Pb bonding between Pb_2Br^{3+} and Pb_2F^{3+} is the weaker Pb–F interaction, which causes the $3a_1$ MO to drop below $2b_1$. The F($2p_z$) atomic orbitals (AOs) thus perturb less the partial Pb–Pb bond; $2a_1$ becoming less and $3a_1$ more Pb–Pb bonding. The effect is largest for the antibonding combination of the F($2p_z$) AO, and therefore a net gain in the Pb–Pb bonding going from bridging bromide to fluoride can be observed.

A correlation between the thermodynamic stability of the dilead species, expressed in their overall stability constant β_{21}, and the Pb–Pb overlap population can be observed.

Stability, β_{21}: $OH > I > F > Br \approx Cl$

Pb–Pb overlap population: $OH \approx I \approx F > Br \approx Cl$

Pb–X overlap population: $OH \approx F < I < Br \approx Cl$

The inverse correlation between the thermodynamic stability and Pb–X overlap populations indicates that partial Pb–Pb bonding, rather than any covalent Pb–X bonding, is the significant factor contributing to the stability of the dilead species.

It seems that a central anion forming predominantly ionic Pb–X bonds is an optimum case, where the attractive Pb–X Coulombic interaction brings the Pb_2^{4+} pair close enough for partial Pb–Pb bonding. A more covalently bound central anion slightly rehybridizes the AOs of the lead atoms in the direction of the X, enhancing Pb–X bonding, at the expense of partial Pb–Pb bonding. Again, it is instructive to compare with the electron-rich hypervalent Bi clusters, such as Bi_9^{5+}, which are stable only in extremely acidic media with very poorly Lewis-donating anions

(24) Corbett, J. D. *Prog. Inorg. Chem.* **1976**, *21*, 129–158.
(25) Corbett, J. D. *Chem. Rev.* **1985**, *85*, 383–397.

Table III. Calculated Energetics of Nitrate Bridging

	$Pb_2Br^{3+} - NO_3^-$		$Tl_2Br^+ - NO_3^-$
configuration	ΔE^a/eV	overlap population[b]	ΔE^a/eV
3a	0.68	2	−0.17
3b	1.62	−2	0.22
3c	2.20	5	0.03

[a] Reference state is separate NO_3^- and M_2Br; a negative value corresponds to a stabilization, positive to destabilization. [b] Percent of the standard Pb–Pb bond.

such as $AlCl_4^-$.[24,25] Occasionally, the term "anticoordination chemistry" has been used to describe the bonding in these molecules. This terminology, however, fails to emphasize both the importance of Coulombic interactions and the effect of Al^{3+}.

The general result obtained is that the dilead complexes are stabilized by a partial Pb–Pb bond strong enough to overcome the obvious Pb^{2+}–Pb^{2+} repulsion. This qualitative result is not changed by the inclusion of solvating oxide ions, as in **2a** and **2b**.

Bridging Nitrates. If only Coulombic interactions were relevant there would be no reason to expect the nitrate ions to contribute significantly to the stability of the dilead clusters in a bridging position (in addition to X) rather than in a nonbridging one. The fact that dilead species are not formed in pure nitrate melts further supports this idea.

However, the results obtained for the isoelectronic Tl_2Br^+ complex appear to confuse the issue. The thermodynamic stability for the dithallium is much lower than for the corresponding dilead complex, but the thermodynamic pattern is the same and even more pronounced: $\Delta H^\circ \ll 0$ and $\Delta S^\circ \ll 0$. The structure is, in contrast to the dilead species, bent with a 90° Tl–Br–Tl angle and long Tl–Br and Tl–Tl distances of 3.16 and 4.54 Å, respectively. No significant Tl–Tl bonding and only a weakly covalent Tl–Br interaction is anticipated; this is confirmed by an extended Hückel calculation. Could there be another reason for the additional stability of Tl_2Br^+ relative to TlBr?

We considered bridging nitrates as a possible stabilizing factor for both Pb_2Br^{3+} and Tl_2Br^+. There are three different ways to approach the bent M_2Br structures with a single nitrate ion, as shown in **3a–c**. The results of the calculations are shown in Table

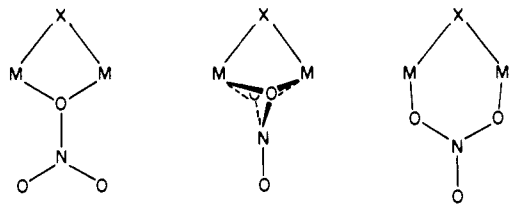

3a **3b** **3c**

III. The metal–oxygen distance was taken as the shortest metal nitrate contact in the corresponding tetranitrato solvate (Pb 2.38 Å; Tl 2.66 Å). In this case we did not do any calculations for oxide solvation models, since any such estimation of stability would have to include the exchange of oxide ions for the bridging nitrate ion. Such a process is highly influenced by Coulombic interactions between nitrates and Pb^{2+}/Tl^+ on one hand and the monovalent solvent cations on the other. There is also a fundamental quantitative difference in energy between a Pb^{2+}–O^{2-} and a Pb^{2+}–ONO_2^- interaction. Since the extended Hückel method does not explicitly treat Coulombic interactions, such comparisons may not be reliable. Furthermore, our prime interest is the difference in covalent interaction between an M_2Br unit and the nitrate ion, going from M = Pb to M = Tl, i.e., spanning the range from significant M–M bonding to where there is essentially none.

The Pb_2Br^{3+} entity is dramatically destabilized by a bridging nitrate, as seen from the results in Table III. The main reason for this bond weakening is a depletion of Pb–Pb bonding. The overlap population decreases from 14% to less than 5% of a standard bond for the different configurations. The Pb–Br bond is also slightly weakened. The absence of a bridging nitrate in the dilead complexes is indicated by thermodynamic, Raman spectroscopic, and X-ray scattering experiments. However, it is always difficult to make good arguments for something you cannot observe.

The Tl_2Br^+ complex is not destabilized in the same way; essentially there is no Tl–Tl bonding to be affected by the rehybridization induced by the bridging nitrate ion. Configuration **3a** is the most stable. This configuration is also the least destabilized in the dilead bromide species.

There exists an interesting analogy between the covalently dibridged $Pb_2BrNO_3^{2+}$ shown in **3a** and mono- and disiloxanes. These silicon compounds form a series of compounds where the Si–Si bonding best is described by structures **4a–c**.[26] Addition

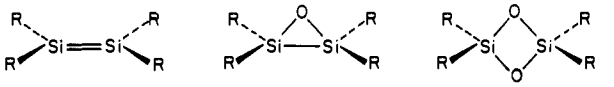

4a **4b** **4c**

of oxygen atoms both oxidizes and rehybridizes the MOs in such a way that the Si–Si bonding is completely annihilated in **4c**. Covalent bridging atoms, anions, or ligands thus are fatal for any metal–metal bonding between main-group elements such as Si and Pb.

We conclude that there exists neither experimental nor theoretical evidence for any bridging nitrate contribution to the stability of the dilead complexes.

Lead Hydroxo/Oxo Clusters

The $Pb_2(OH)_2^{2+}$ complex or cluster deserves special attention for two reasons. First, it is the fundamental structural unit in a number of medium-size lead hydroxo/oxo clusters. Second, it carries the potential of two extreme covalent bonding schemes in a square unit, as indicated in **5a** and **5b**. The former (Pb–Pb

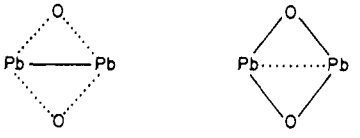

5a **5b**

bonding) seems to dominate in an ionic liquid medium and concentrated aqueous solution and the latter (no significant Pb–Pb bonding) in the solid state (vide infra).

Due to the long Pb–O(H) distances in $Pb_2(OH)_2^{2+}$ the orientation of the OH group does not affect the MOs of interest in the complex. The structures of $Pb_4(OH)_4^{4+}$ (**6a**) and $Pb_6O(OH)_6^{4+}$ (**6b**), as determined by X-ray scattering and Raman spectroscopy, exhibit bonding similar to that of **5a** in concentrated aqueous solution.[27–33] The Pb–O(H) distance is 2.6 Å, and the

(26) Only a few examples of experimental structures, NMR studies, and theoretical calculations taken from the vast literature on this subject are given here. Please consult the references of the later papers cited for a more complete review. (a) Almenningen, A.; Bastiansen, O.; Ewing, V.; Hedberg, K.; Traettberg, M. *Acta Chem. Scand.* **1963**, *17*, 2455–2460. (b) Glidewell, C.; Liles, D. C. *Acta Crystallogr., Sect. B* **1978**, *34*, 119–124. (c) Glidewell, C.; Liles, D. C. *Acta Crystallogr., Sect. B* **1978**, *34*, 124–128. (d) Barrow, M. J.; Ebsworth, E. A. V.; Harding, M. M. *Acta Crystallogr., Sect. B* **1979**, *35*, 2093–2099. (e) Fink, M. J.; Haller, K. J.; West, R.; Michl, J. *J. Am. Chem. Soc.* **1984**, *106*, 822–823. (f) Michalczyk, M. J.; Fink, M. J.; Haller, K. J.; West, R.; Michl, J. *Organometallics* **1986**, *5*, 531–538. (g) Yokelson, H. B.; Millevolte, A. J.; Adams, B. R.; West, R. *J. Am. Chem. Soc.* **1987**, *109*, 4116–4118. (h) Boatz, J. A.; Gordon, M. S. *J. Phys. Chem.* **1989**, *93*, 3025–3029. (i) Schmidt, M. W.; Nguyen, K. A.; Gordon, M. S.; Montgomery, J. A., Jr. *J. Am. Chem. Soc.* **1991**, *113*, 5998–6001.

(27) Esval, O. E. Ph.D. Thesis, University of North Carolina, 1962.

(28) Johansson, G.; Olin, Å. *Acta Chem. Scand.* **1968**, *22*, 3197–3201.

(29) Maroni, V. A.; Sprio, T. G. *J. Am. Chem. Soc.* **1967**, *89*, 45–48.

peaks from Pb–Pb distances in the radial distribution functions are very wide, with an average Pb–Pb separation of 3.85 Å. The wide peaks indicate that several distinct Pb–Pb contacts ranging between 3.4 and 4.1 Å contribute, rather than a single Pb–Pb interaction at the average distance with a wide dispersion. This is further supported by the observation of low-frequency peaks in the Raman spectra of such solutions and in the solid state. Such bands are more readily interpreted in terms of the vibrational stretching modes of a covalent Pb–Pb partial bond, rather than the bending mode of the ionic Pb–O(H)–Pb unit.[34] The former is more likely to induce changes in the polarizability of the cluster than the latter, and Raman spectroscopy is only sensitive to vibrational modes which change the polarizability of a molecular unit.

Calculations were performed on the isolated clusters. These clusters, $Pb_4(OH)_4^{4+}$ (**6a**), $Pb_6O(OH)_6^{4+}$ (**6b**), and $Pb_6O_4(OH)_4$ (**6c**), seem to follow the other bonding scheme, **5b**, in which there

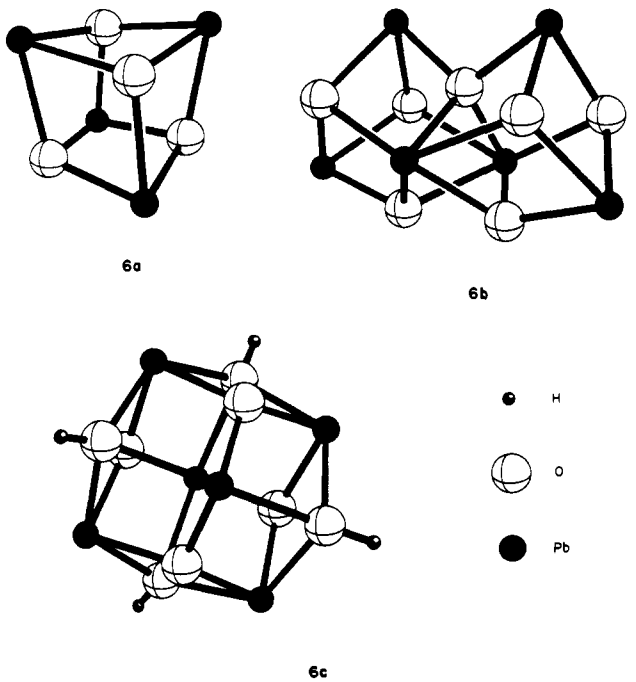

is little Pb–Pb bonding. Their structural characteristics are shown in Table IV; they all have short Pb–O/OH distances and fairly long Pb–Pb contacts. Consistent with our findings for the solution dilead species, significant Pb–Pb bonding is neither anticipated nor found. The reason that the larger lead hydroxo/oxo clusters show little lead–lead bonding, as in **5b**, in contrast to what is found in solution, has to be ascribed to the lack of a stabilizing ionic medium.

The $Pb_6O_4(OH)_4$ cluster **6c** is an M_6X_8 cluster. Such entities are readily formed by the early (and a few late) transition elements, e.g., $Mo_6Cl_8^{4+}$ and the fundamental structural unit of the potentially superconducting Chevrel–Sergent phases $A_2Mo_6S_8$.[43-45]

Table IV. Calculated Overlap Populations in Various Lead Hydroxo/Oxo Clusters

	cluster	$d_{Pb-O/OH}$/Å	d_{Pb-Pb}/Å	overlap population$_{Pb-Pb}$[a]	ref
6a	$Pb_4(OH)_4^{4+}$	2.34–54	3.72–94	0	35, 36[b]
6b	$Pb_6O(OH)_6^{4+}$	2.24–82	3.46–4.06	0–4	37, 38[c]
6c	$Pb_6O_4(OH)_4$	2.20–49	3.67–71	0	39
7a	$Pb_8O_4^{8+}$	2.23–37	3.55–4.04	0–4	40
7b	$Pb_6O_2^{8+}$	2.21–45	3.57–4.01	0–9	41
7c	Pb_4O^{6+}	2.20–36	3.70–82	1–5	42

[a] Percent of a standard Pb–Pb bond. [b] The data from ref 36 used. [c] The data from ref 37 used.

The transition-metal clusters have an octahedral M_6 core, with significant M–M bonding, surrounded by eight ligands capping the faces. The ligands form a more or less regular cube around the M_6 core.

Clusters **7a–c** represent intermediate states in which the relation between the square Pb_2O_2 and tetrahedral Pb_4O units can be seen. It is clear that the tetrahedron would favor Pb–Pb bonding since only one oxygen atom bridges the lead atoms. However, in α- and β-PbO, which are the model structures for almost all the solid-state chemistry of divalent lead oxide, the tetrahedra are linked via edges into infinite two-dimensional layers. This results in a structure where all lead atoms are linked by two oxide bridges at a short Pb–O separation of 2.3 Å. In spite of this fact, Trinquier and Hoffmann showed that both intra- and interlayer Pb–Pb interactions do influence both the structural and physical properties of the divalent lead oxides.[12]

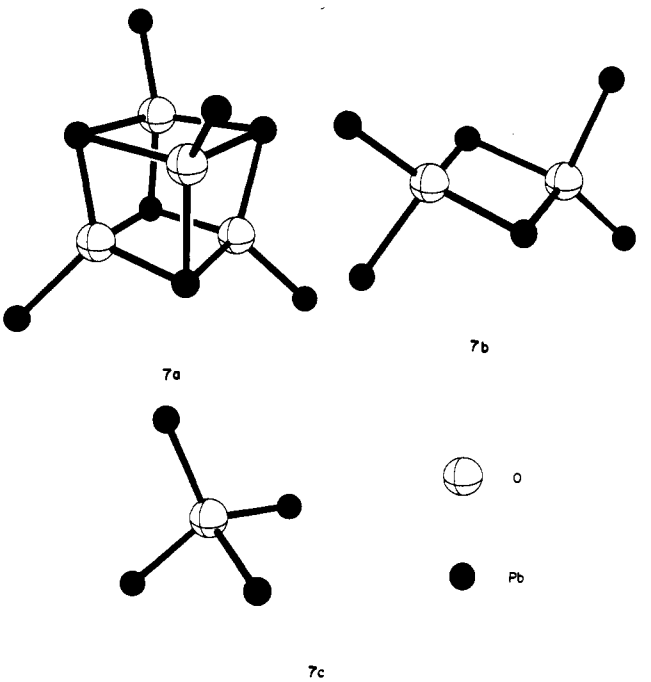

Square Pb_2O_2 Layers in Extended Structures

Square Pb_2O_2 units forming planar layers are found in a new type of high-temperature superconductor. The $[(PbO)_2Cu]$-$YSr_2Cu_2O_6$ family exhibits superconductivity up to $T_c \approx 70$ K when oxidized by an exchange of Y^{3+} or other lanthanoids for Ca^{2+} or Ba^{2+}.[3,46-55] The parent compound is a semiconductor. The structure is slightly distorted orthorhombic; in the calculations

(30) Maroni, V. A.; Spiro, T. G. *Inorg. Chem.* **1968**, *7*, 188–192.
(31) Spiro, T. G.; Maroni, V. A.; Quicksal, C. O. *Inorg. Chem.* **1969**, *8*, 2524–2526.
(32) Spiro, T. G. *Prog. Inorg. Chem.* **1970**, *11*, 1–51.
(33) Tsai, P.; Coney, R. P. *J. Chem. Soc., Dalton Trans.* **1976**, 1631–1634.
(34) Bengtsson, L. A.; Brooker, M. H., to be published.
(35) Hong, S.-H.; Olin, Å. *Acta Chem. Scand.* **1973**, *27*, 2309–2320.
(36) Hong, S.-H.; Olin, Å. *Acta Chem. Scand., Ser. A* **1974**, *28*, 233–238.
(37) Olin, Å.; Söderquist, R. *Acta Chem. Scand.* **1972**, *26*, 3505–3514.
(38) Spiro, T. G.; Templeton, D. H.; Zalkin, A. *Inorg. Chem.* **1969**, *8*, 856–861.
(39) Hill, R. J. *Acta Crystallogr., Sect. C* **1985**, *41*, 998–1003.
(40) Keller, H.-L. *Z. Anorg. Allg. Chem.* **1982**, *491*, 191–198.
(41) Sterns, M.; Parise, J. B.; Howard, C. J. *Acta Crystallogr., Sect. C* **1986**, *42*, 1275–1277.
(42) Behm, *Acta Crystallogr., Sect. C* **1983**, *39*, 1317–1319.
(43) Wheeler, R. A.; Hoffmann, R. *J. Am. Chem. Soc.* **1986**, *108*, 6605–6610.
(44) Wheeler, R. A.; Hoffmann, R. *J. Am. Chem. Soc.* **1988**, *110*, 7315–7325.
(45) Mingos, D. M. P.; Wales, J. D. *Introduction to Cluster Chemistry*; Pergamon Press: Englewood Cliffs, 1990.
(46) Subramanian, M. A.; Gopalakrishnan, J.; Torardi, C. C.; Gai, P. L.; Boyes, E. D.; Askew, T. R.; Flippen, R. B.; Farneth, W. E.; Sleight, A. W. *Physica C* **1989**, *157*, 124–130.
(47) Cava, R. J.; Marezio, M.; Krajewski, J. J.; Peck, W. F., Jr.; Santoro, A.; Beech, F. *Physica C* **1989**, *157*, 272–278.

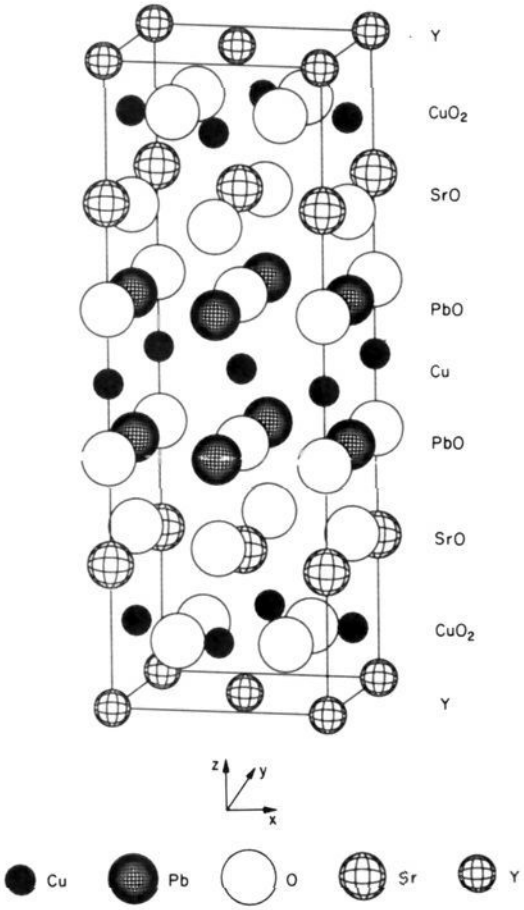

Figure 2. Crystallographic unit cell of $[(PbO)_2Cu]YSr_2Cu_2O_6$.

it is approximated as tetragonal, with cell parameters $a = 5.3933$, $b = 5.4311$, and $c = 15.7334$ Å.

The unit cell is shown in Figure 2. The notations used are consistent with those introduced by Cava, Batlogg, and co-workers at the AT&T Bell Laboratories.[13,47,51] In order to gain an understanding of the chemical bonding, electronic structure, and the role played by the planar Pb_2O_2 layers in the three-dimensional structure, we start with the Pb_2O_2 unit. Then, step by step, we build up the complete structure, analyzing any new features encountered during the process.

In an ideal Pb_2O_2 layer in this family of compounds, the average Pb–O distance is 2.70 Å and the Pb–Pb distance is 3.85 Å. These facts indicate that both the Pb–O and Pb–Pb intralayer interactions are weak and predominantly electrostatic in character. The energy diagram in Figure 3 confirms these expectations. The formation of a one-dimensional chain of Pb_2O_2 units introduces little new (see Figure 3). The energy gap between filled and unfilled bands in the extended structure is in the range of 4–5 eV.

The stepwise construction of the central PbO–Cu–PbO triple layer, as shown in **8a–c**, includes extension to two dimensions,

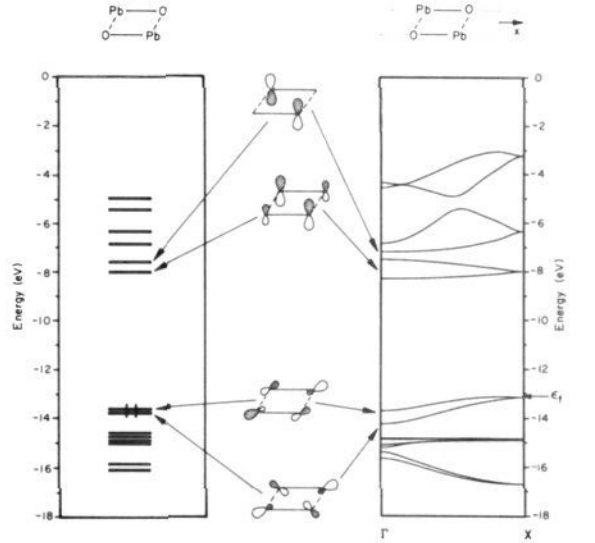

Figure 3. Energy diagram of a molecular Pb_2O_2 unit and the band structure of a chain of such units, together with analogous MOs and COs at Γ near the Fermi level.

attachment of axial oxygens O(1) at a distance of 2.153 Å on each Pb atom in order to simulate the connection to the potentially superconducting CuO_2 sheets, and displacement of the Pb atoms out of the O(2) plane toward the Cu(1) layer by 0.053 Å, **8a**.

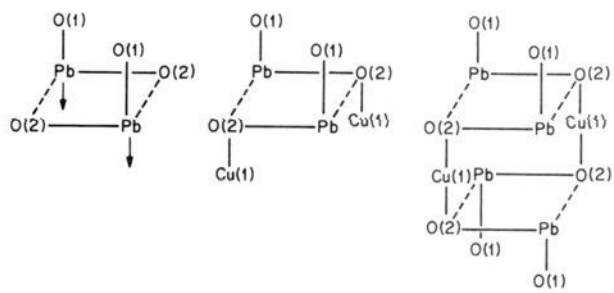

8a **8b** **8c**

These modifications introduce also little new in terms of the electronic structure. There is still a gap of 4 eV between the filled and unfilled bands. Attachment of the Cu(1) atoms under the Pb_2O_2 layer **8b** gives two new bands in the middle of the gap, primarily of $Cu(3d_{z^2},4p_z)$–$O(2p_z)$ bonding character. However, upon proceeding to the complete triple layer **8c**, these bands mix further with the O(2) atoms of the lower Pb_2O_2 layer to give bonding bands far below the Fermi level and antibonding ones far above.

In the two-dimensional slab **8c** the Pb atoms in the upper and lower Pb_2O_2 layers are brought as close together as 3.515 Å. The Pb atoms are not supported by any bridging oxides, and a strong Pb–Pb interaction is expected on the basis of the knowledge acquired for molecular dilead entities.

The band structure with crystal orbitals (COs) at Γ near the Fermi level, density of state (DOS), and crystal orbital overlap population (COOP) for the Pb atoms and interlayer Pb–Pb interactions are displayed in Figure 4.[56] The COs retain their primary character all the way through the Brillouin zone, although AOs from Cu(1), O(1), and O(2) mix with the COs seen at Γ. The electronic gap around the Fermi level becomes completely occupied by bands of essentially weakly Pb–O(1) σ antibonding (A, B) and bonding (C, D) and strongly interlayer Pb–Pb σ bonding (A, B) and antibonding (C, D) bands. The capping

(48) Fu, W. T.; Zandbergen, H. W.; Haije, W. G.; De Jongh, L. J. *Physica C* **1989**, *159*, 210–214.
(49) Tokiwa, A.; Oku, T.; Nagoshi, M.; Kikuchi, M.; Hiraga, K.; Syono, Y. *Physica C* **1989**, *161*, 459–467.
(50) Cava, R. J.; Bordet, P.; Capponi, J. J.; Chaillout, C.; Chenavas, J.; Fournier, T.; Hewat, E. A.; Hodeau, J. L.; Levy, J. P.; Marezio, M.; Batlogg, B.; Rupp, L. W., Jr. *Physica C* **1990**, *167*, 67–74.
(51) Marezio, M.; Santoro, A.; Capponi, J. J.; Hewat, E. A.; Cava, R. J.; Beech, F. *Physica C* **1990**, *169*, 401–412.
(52) Nakabayashi, Y.; Imoto, S.; Hibiya, T.; Satoh, T.; Kubo, Y. *Mol. Cryst. Liq. Cryst.* **1990**, *184*, 171–175.
(53) Gopalakrishnan, J. In *Chemistry of High Temperature Superconductors*; Rao, C. N. R., Ed.; World Scientific: Singapore, 1991; pp 156–185.
(54) Jørgensen, J.-E.; Andersen, N. H. *Acta Chem. Scand.* **1992**, *46*, 122–125.
(55) Jørgensen, J.-E.; Andersen, N. H. *Acta Chem. Scand.* **1991**, *45*, 19–22.
(56) Hoffmann, R. *Solids and Surfaces: A Chemist's View on Bonding in Extended Structures*; VCH: New York, 1988.

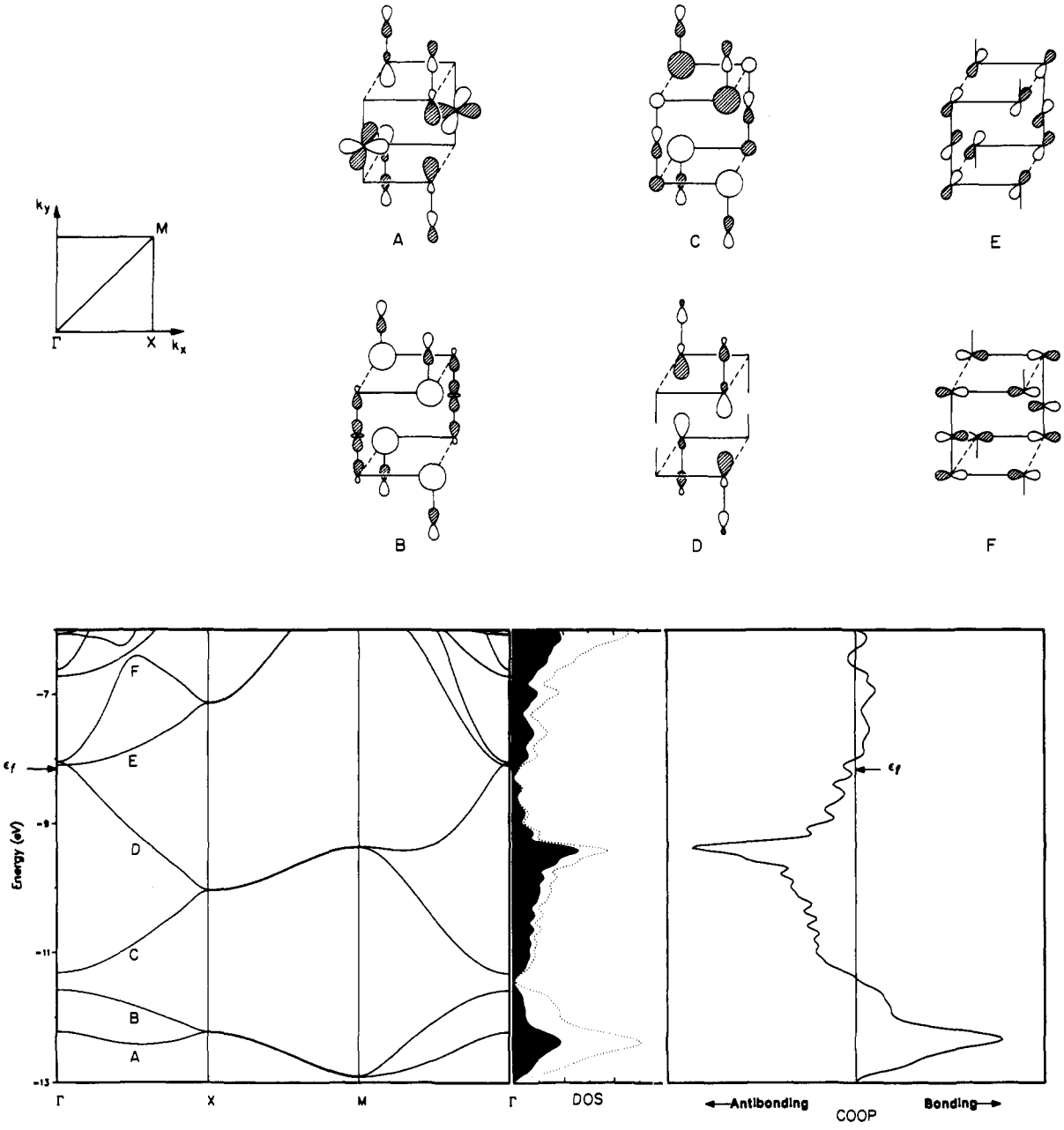

Figure 4. Brillouin zone, band structure, and COs near the Fermi level of the central triple layer according to **8c**. The band structure is expanded in the region −13 to −6 eV and compared with the Pb projection and total DOS and the interlayer Pb–Pb COOP.

O(1)s were provided with hydrogen atoms at a distance of 0.988 Å in order to simulate the effect of the whole three-dimensional structure. No significant changes were observed in the results. The computational results of **8c** are shown in Table V. The band structure obtained is consistent with the compound $[(PbO)_2Cu]$-$YSr_2Cu_2O_6$ being at least a semiconductor.

The interlayer Pb–Pb COOP is only 4% of a standard Pb–Pb bond, which is clearly explained by Figure 4. The Fermi level is so high that both the bonding and antibonding bands are completely filled, leaving essentially no net Pb–Pb bonding. The maximum COOP is about 42% of a standard bond at −11.3 eV, but the actual Fermi level is much higher. The HOMO and LUMO of the ideal unit cell treated as a molecule are analogous to the COs D and E in Figure 4.

The experimental picture is not as simple as this; the crystal structure, as determined by neutron scattering of a powder sample, reveals a superstructure with a geometrical grouping of four oxygen atoms (**9**) of the O(2) oxygen atoms, i.e., in the Pb_2O_2 layers.

There exists one more restriction on the possible geometries which dramatically decreases the number of spatial arrangements;

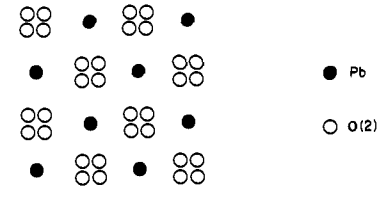

9

each lead atom is surrounded by four O(2) atoms at 2.33, 2.45, 3.00, and 3.13 Å. The possible realizable geometries can be denoted as island, chain, and zigzag distortions, similar to those discussed for the planar Bi_2O_2 and Tl_2O_2 layers in other high-T_c superconductors and in the square network of GdPS.[57,58] The fact that we have two symmetry-equivalent Pb_2O_2 layers makes things a bit more complicated. We will confine our investigation to the three distortions either in an "eclipsed" or "staggered"

(57) Torardi, C. C.; Jung, D.; Kang, D. B.; Ren, J.; Whangbo, M.-H. *Mat. Res. Soc. Symp. Proc.* **1989**, *156*, 295–308.
(58) Tremel, W.; Hoffmann, R. *J. Am. Chem. Soc.* **1987**, *109*, 124–140.

Table V. Interactions and Charges in the PbO–Cu–PbO Triple Layers

interaction	ideal	**10a**	**10b**	**10c**	**11a**	**11b**	**11c**
			Overlap Populations[a]				
Cu(1)–O(2)	0.320	0.266	0.269	0.258	0.267	0.262	0.258
Pb–O(2)	0.021	0.137	0.053	0.114	0.062	0.056	0.115
Pb–O(1)	0.232	0.238	0.237	0.243	0.242	0.246	0.245
Pb–Pb(intra)	0.007	–0.038	0.005	–0.018	0.009	0.005	–0.019
Pb–Pb(inter)	0.027	0.026	0.017	0.043	0.065	0.075	0.060
Pb–Cu(1)	–0.001	0.002	0.012	0.009	0.019	0.020	0.012
			Charges				
Cu(1)	+0.43	+0.42	+0.40	+0.34	+0.38	+0.34	+0.34
Pb	+1.57	+1.52	+1.52	+1.54	+1.53	+1.54	+1.54
O(1)	–1.77	–1.77	–1.77	–1.77	–1.77	–1.77	–1.77
O(2)	–1.51	–1.46	–1.45	–1.44	–1.45	–1.45	–1.44

[a] Reduced absolute values.

Table VI. Comparison of Stability Between Two-Dimensional Distortions

distortion	ΔE^a/eV	distortion	ΔE^a/eV
10a	–1.47	**11a**	–2.00
10b	+0.19	**11b**	–0.56
10c	–0.71	**11c**	–1.13

[a] Energy relative to the ideal two-dimensional structure **8c**; negative values represent a stabilization, positive ones a destabilization.

mode, as illustrated in **10a–c** and **11a–c**; this will be sufficient to survey possible effects on the band structure.

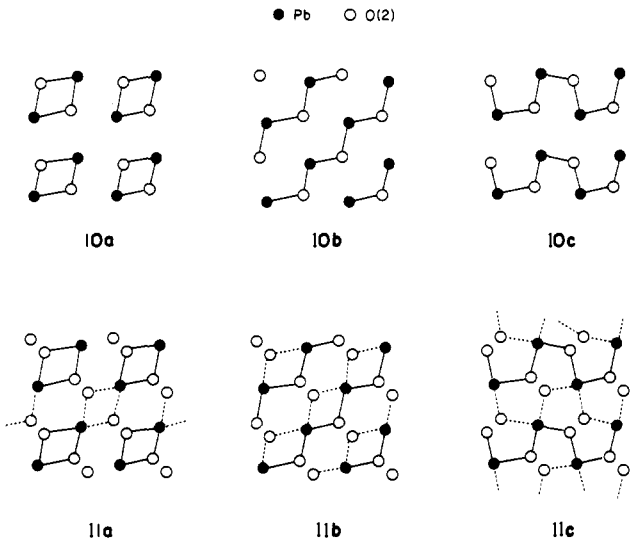

The results are displayed in Table V. The band structures change quantitatively but *not* qualitatively; the COs about the Fermi level retain their character, although some AOs from Cu(1), O(1), and O(2) mix in due to the distortions. The Pb–Pb bonding and antibonding contributions to these bands remain the predominant feature. The stability of the different distortions relative to the ideal structure is given in Table VI. The staggered island configuration seems to be the most stable. In fact, in two recent publications on the analogous compounds $[(PbO)_2Cu]$-$Ho_{0.625}Ca_{0.375}Sr_2Cu_2O_6$ and $[(PbO)_2Cu]HoSr_2Cu_2O_6$ were shown to have Pb_2O_2 layers with staggered island distortion.[54,55]

However, the calculations performed on the full three-dimensional structure were confined to ideal Pb_2O_2 layers. The distortions introduce such small qualitative changes that the ideal structure serves as a good model for detection of the changes upon oxidation, reduction, and substitutions.

Before discussing the results of the three-dimensional structure, a few comments on the so-called inert-pair (or stereochemically active 6s lone-pair) effect should be made. As seen in Figure 4, the COs involving Pb–Pb σ bonding or antibonding properties show the Pb_2O_2 layers to have (6s,6p)-type lobes pointing into the void of the Cu(1) layer. The HOMO of an extended Hückel calculation on the PbO_5^{8-} fragment **12** shows the lone pair explicitly. The HOMO consists of a hybridized MO of sp^x-type,

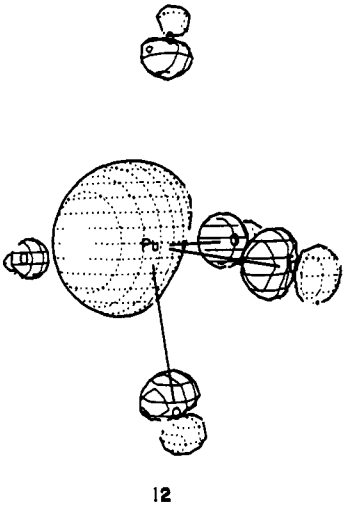

12

pointing away from the three short Pb–O bonds in a manner analogous to that in NH_3. The lone pairs are directed toward the opposite Pb_2O_2 layer, however, at an angle relative to the unit cell z-axis.

The band structure of the ideal three-dimensional compound with the unit cell of Figure 2 is very similar to that of the capped ideal triple layer (**8c**, Figure 4). The new features are displayed in Figure 5; it can be seen that four new flat bands about –12 eV have appeared. These bands are mainly composed of $Cu(d_{xy})$–$O(2s,2p_x,2p_y)$ interactions between Cu(2) and O(3) in the potentially superconducting CuO_2 sheets. The Fermi level has gone down in energy by almost 3 eV to about –11.3 eV. The new Cu(2)–O(3) σ antibonding bands give the greatest contribution to the DOS at the Fermi level. There is also a significant contribution from Pb.

The results summarized in Table VII show that Cu(2) essentially is reduced by Pb to an oxidation state close to that of the Cu(1) atoms. This is the reason for the decrease in energy of the Fermi level. The oxidation of the Pb atoms is expected to give stronger bonding between the Pb_2O_2 layers, since the Pb–Pb antibonding bands will be depopulated. The COOP of Figure 5 confirms these anticipations. The strong interlayer Pb–Pb bonding explains the 0.051 Å displacement of the Pb atoms out of the O(2) layer toward the opposite Pb_2O_2 sheet.

The tight-binding approximation predicts $[(PbO)_2Cu]$-$YSr_2Cu_2O_6$ to be a metallic conductor with partly filled bands of Cu(2), O(3), and Pb character. The compound is, however, a semiconductor. This effect is attributed to localization of the Cu(2) states in the CuO_2 sheets.[53,59–61] Because it does not include electron repulsion, the extended Hückel formalism cannot distinguish between localized states (Mott insulators) and actual conductors.

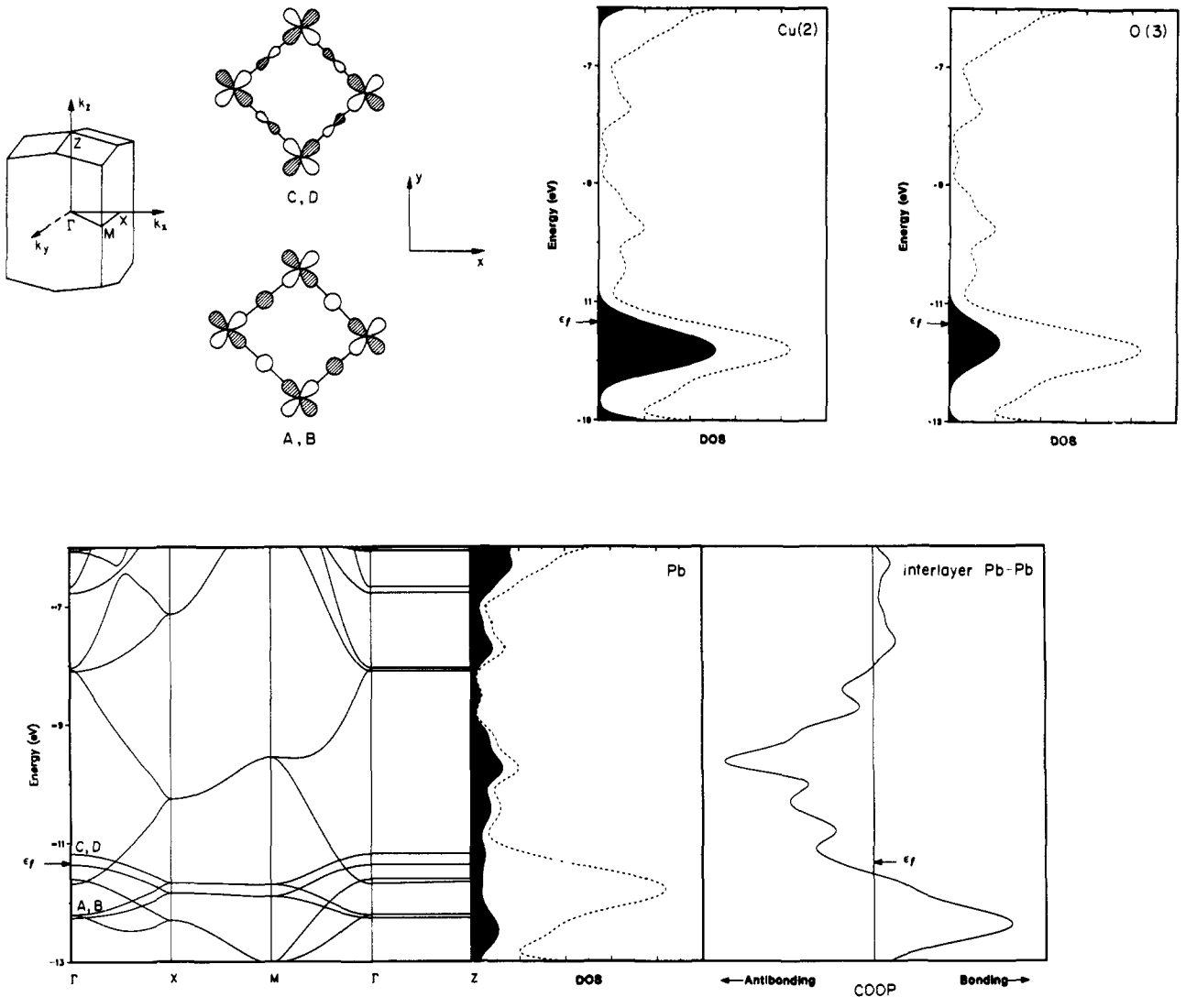

Figure 5. Brillouin zone, band structure, and new COs in the ideal three-dimensional structure. The band structure is expanded in the region −13 to −6 eV and compared with the projections of Pb, Cu(2), and O(3) and total DOS together with the COOP of the interlayer Pb–Pb interaction.

The localized states can be disrupted by mild oxidation of the CuO_2 sheets, upon replacement of a fraction of the Y^{3+} ions for Ca^{2+}.[59-61] The results of a $(Y_{0.5}, Ca_{0.5})^{2.5+}$ substitution are shown in Table VII. The band structure remains almost unchanged, but slight oxidation of Cu(2) can be observed.

The idea of a one-way charge transfer has been put forward, where oxidation of the CuO_2 sheet, but not oxidation of Cu(1) by inclusion of interstitial oxygen atoms, induces superconductivity.[47,51,53] The idea relies on the generally accepted importance of a oxidized or disproportionation-facilitated CuO_2 sheet to form a low concentration of Cu(III) atoms.[59,60] The one-way oxidation is based on valence estimates of the Cu(2) atoms from bond length arguments; this is the so-called local charge model. However, in our calculations no such unidirectionality, which seems to us unchemical, appears to exist. On the contrary, the inclusion of interstitial oxygen atoms into the Cu(1) layer oxidizes the CuO_2 sheet probably to a too large extent. Thus the optimum conditions for a Cu(II)/Cu(III) mixed valence state are disrupted. Rather than no oxidation of the CuO_2 sheet at all, this seems to be the case.

Occupancies of 25 and 100% by interstitial oxygen atoms, O(ist), in the Cu(1) layer were considered. The O(ist)s were placed to form linear Cu(1)–O(ist)–Cu(1) chains analogous to those in the CuO_2 sheets. The Cu(1)–O(ist) and Pb–O(ist) distances are thus 1.914 and 2.598 Å, respectively. The Pb atoms and interstitial oxygen atoms form bent Pb–O(ist)–Pb entities, resembling the dilead complexes observed in ionic liquids **5a**. The Pb–O(ist) interactions form essentially bonding and antibonding bands, pushed down and up and out of the region about the Fermi level. In Figure 6 the tendency is shown with arrows for a 25% O(ist) occupancy and is completed for the 100% occupancy. The bands crossing the Fermi level thus contain no Pb contribution at all. This is seen in the band structures and DOS in Figure 6. New bands of Cu(1)–O(ist) character, analogous to those from the CuO_2 sheets, appear near the Fermi level, as well as a pair of bands of essentially Cu(1)–O(2) σ antibonding character, of $Cu(3d_{z^2})$–$O(2s,2p_z)$ origin. The DOS shows the separation in energy between the contributions from the Cu(1) and Pb atoms (Pb contributing nothing to DOS near the Fermi level) and how O(ist) is distributed between both bands.

The inclusion of interstitial oxygen atoms initially oxidizes Cu(1) and Pb, but as the Pb-containing bands are lifted above the Fermi level the oxidation starts to affect also Cu(2).

The effect of substitution of Pb for Bi and Tl is shown in Table VII and Figure 7. The substitutional atoms are placed in the Pb_2O_2 layers so that the Pb atoms always have a substituted atom in the identical position in the opposite layer. A $(Pb_{0.5}, Bi_{0.5})^{2+}$ and $(Pb_{0.5}, Tl_{0.5})^{2+}$ state represents both changes in parameters and the total number of electrons. The substitution for Bi gives a downshift of the Pb/Bi bands relative to the purely Pb ones.

(59) Sleight, A. W. In *Chemistry of High-Temperature Superconductors*; Nelson, D. L., Whittingham, M. S., George, T. F., Eds.; American Chemical Society: Washington DC, 1987; pp 2–12.
(60) Sleight, A. W. *Science* **1988**, *242*, 1519–1527.
(61) Burdett, J. K.; Kulkarni, G. V. *Phys. Rev.* **1989**, *40*, 8908–8932.

Table VII. Some Calculated Bonding Parameters for the $[(PbO)_2Cu]YSr_2Cu_2O_6$ Compound

interaction	ideal	Ca^{2+}-exchange	$Cu(1)O(ist)_{1/2}$	$Cu(1)O(ist)_2$	Bi-subst[b]	Tl-subst[c]
			Overlap Populations[a]			
Cu(1)–O(2)	0.323	0.323	0.306	0.308	0.339	0.330
Cu(2)–O(1)	0.032	0.032	0.032	0.032	0.031	0.033
Cu(2)–O(3)	0.182	0.198	0.187	0.187	0.178	0.199
Pb–O(1)	0.365	0.365	0.365	0.380	0.313	0.347
Pb–O(2)	0.079	0.079	0.084	0.088	0.061	0.083
Pb–Pb(intra)	0.010	0.010	-0.001	0.009	0.021	0.004
Pb–Pb(inter)	0.315	0.315	0.262	0.015	0.110	0.295
Cu(1)–O(ist)			0.195	0.157		
Pb–O(ist)			0.063	0.113		
			Charges			
Cu(1)	+0.42	+0.42	+0.59	+0.30	+0.46	+0.54
Cu(2)	+0.27	+0.42	+0.32	+1.27	+0.24	+0.43
Pb	+2.20	+2.20	+2.31	+2.70	+1.66	+1.94
Bi					+3.09	+2.04
Tl						
Sr	+1.97	+1.98	+1.98	+2.00	+1.93	+2.01
Y	+2.79	+2.80	+2.79	+2.79	+2.79	+2.79
Ca		+1.78				
O(1)	-1.58	-1.58	-1.57	-1.54	-1.62	-1.66
O(2)	-1.32	-1.32	-1.32	-1.26	-1.38	-1.40
O(3)	-1.58	-1.52	-1.56	-1.56	-1.58	-1.52
O(ist)			-1.20	-1.11		
			Fermi Levels/eV			
	-11.341	-11.506	-11.345	-11.341	-10.961	-11.508

[a] Reduced absolute values. [b] Half of all Pb exchanged for Bi; all interactions involving Pb are actually Pb/Bi. [c] Half of all Pb exchanged for Tl; all interactions involving Pb are actually Pb/Tl.

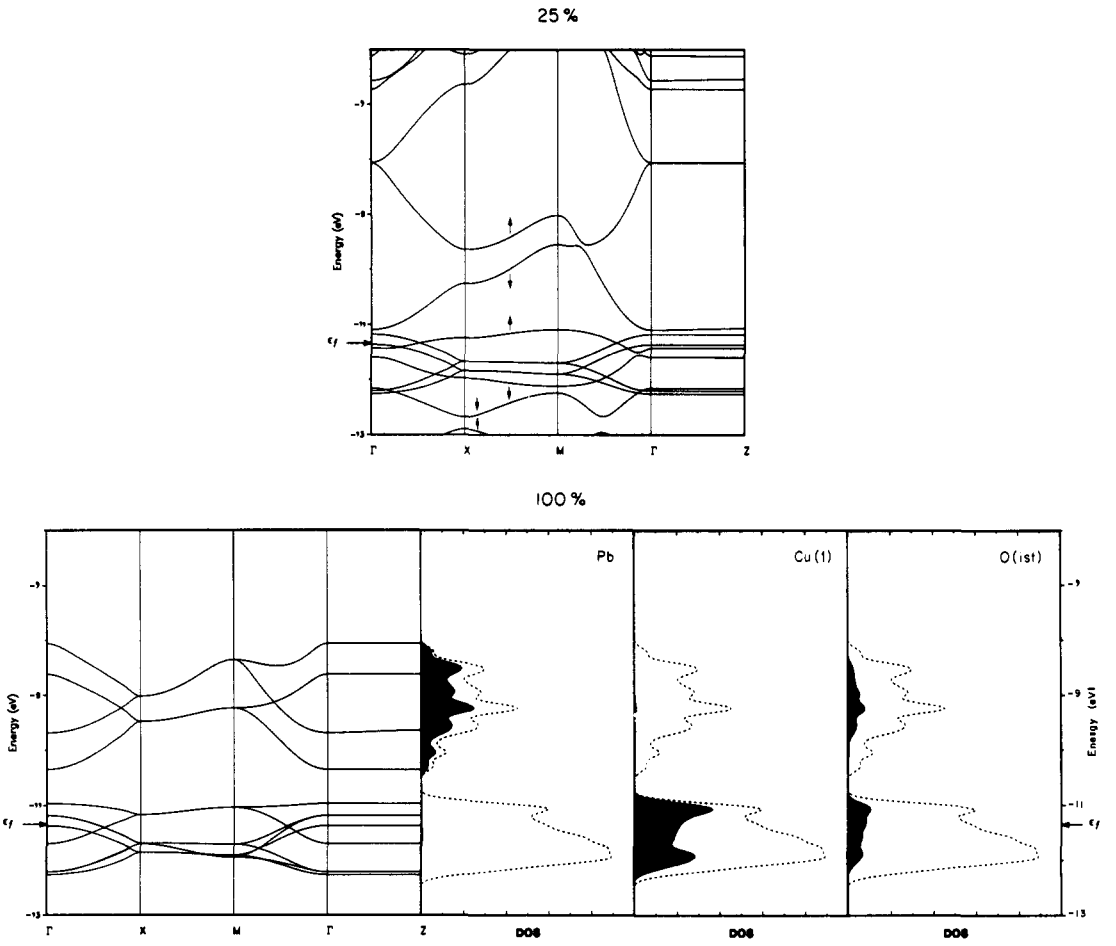

Figure 6. Effect of interstitial oxygen O(ist) at 25 and 100% occupancy of the sites in the Cu(1) layer. The band structure at 100% occupancy is compared with the projected DOSs of Pb, Cu(1), and O(ist).

The bands are more narrow and thus contribute more to the DOS at the Fermi level. Since the system contains more electrons, the Pb/Bi antibonding bands are slightly populated, and thus the interlayer Pb–Bi bonding is weakened.

On the other hand, the substitution for Tl gives an upshift of the Pb/Tl bands, especially of the Pb–Tl antibonding ones. Since the system contains less electrons, the bonding Pb–Tl bands are slightly depopulated but the Pb–Tl interlayer bonding is strong.

The Pb_2O_2 layers in the above mentioned superconductor relate directly to another family of superconductors consisting of infinite

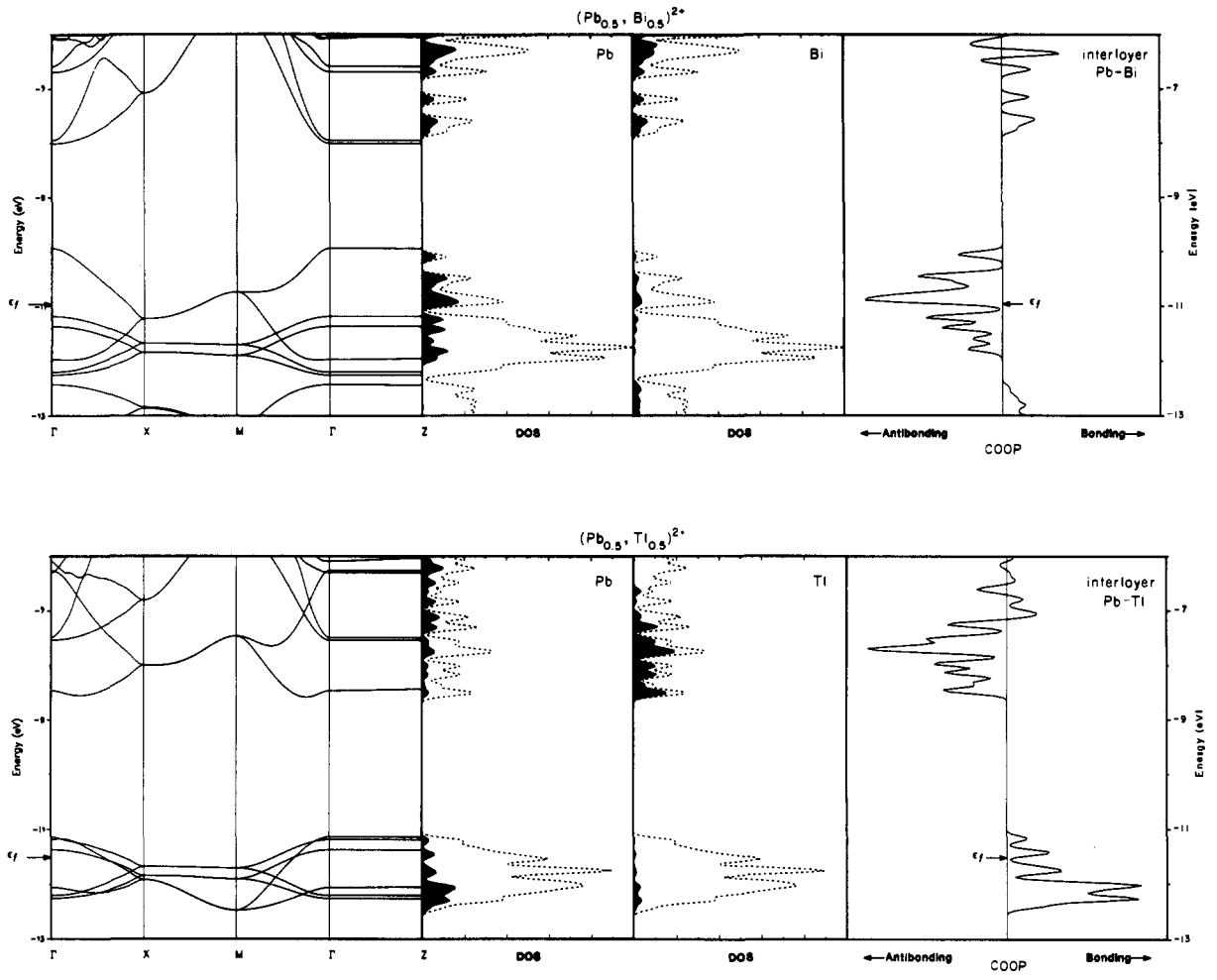

Figure 7. Band structure of the $(Pb_{0.5},Bi_{0.5})^{2+}$ and $(Pb_{0.5},Tl_{0.5})^{2+}$, Pb and Bi/Tl projected DOSs with the interlayer Pb–Bi/Tl bonding visualized in terms of COOPs.

$(Pb/Bi)O_2$ chains extending in three dimensions, $BaPb_{1-x}Bi_xO_3$.[59,60,62,63] The chains can be formed by letting Pb_2O_2 layers extend into three dimensions, removing every second lead atom, and decreasing the Pb–O distance to about 2.0 Å. Lead is here obviously present in oxidation state +IV, and the structure can be thought of as an extreme case of the bridging bonding scheme **5b**.

Divalent lead in an analogous two-dimensional structure of $(RNH_3)PbI_4$ has also been reported.[64] The idea of substituting the oxides for halides is not new, and examples of halide-containing systems related to this work can be given.[50,65]

Concluding Remarks

In dilead complexes a short Pb–Pb contact and substantial partial bonding stabilize the molecular entities. The role of the anion is to bring the lead ions close enough for the partial Pb–Pb bond to be formed. A predominantly ionic Pb–X interaction is the optimum case for the effect to be realized, since the Pb–Pb bonding MOs only are slightly turned away from the Pb–Pb axis by rehybridization. This bonding scheme extends to medium-size lead hydroxo/oxo clusters in concentrated aqueous solution.

When isolated in the solid state, without any supporting ionic medium, the medium-size clusters exhibit another bonding scheme with strong bridging hydroxides/oxides and short Pb–O(H) distances. Pb–Pb bonding contributes little to the stability of these clusters.

The planar layers consisting of square Pb_2O_2 units in the $[(PbO)_2Cu]YSr_2Cu_2O_6$ family of high-T_c superconductors have little intralayer Pb–Pb bonding, although the Pb–O distances are fairly long. The two Pb_2O_2 layers in the unit cell, bridged by Cu atoms, are close enough to form strong interlayer Pb–Pb bonds. The interlayer Pb–Pb bonding strongly affects the structure, electronic properties, and redox chemistry of this type of ceramic.

Acknowledgment. L.A.B. wishes to thank Thanks to Scandinavia, Inc. and Kungliga Fysiografiska Sällskapet i Lund for their financial support of his stay in R.H.'s research group at Cornell University. The work at Cornell was supported by National Science Foundation Research Grant CHE8912070. We are grateful to Jane Jorgensen for her expert drawings and to Davide Proserpio and Carlo Mealli for providing us with HP- and PC-versions of CACAO.[66]

(62) Sleight, A. W. In *Chemistry of Oxide Superconductors*; Rao, C. N. R., Ed.; Blackwell Scientific: Oxford, 1988; pp 27–33.
(63) Batlogg, B.; Cava, R. J.; Schneemeyer, L. F.; Espinosa, G. P. *IBM J. Res. Develop.* **1989**, *33*, 208–214.
(64) Calabrese, J.; Jones, N. L.; Harlow, R. L.; Herron, N.; Thorn, D. L.; Wang, Y. *J. Am. Chem. Soc.* **1991**, *113*, 2328–2330.
(65) Baeriswyl, D.; Bishop, A. R. *Phys. Scr.* **1987**, *T19*, 239–245.
(66) Mealli, C.; Proserpio, D. M. *J. Chem. Educ.* **1990**, *67*, 399–402.